International Journal of Mass Spectrometry 377 (2015) 410–420

Contents lists available at ScienceDirect

International Journal of Mass Spectrometry

journal homepage: www.elsevier.com/locate/ijms

40 years of Fourier transform ion cyclotron resonance mass spectrometry

Alan G. Marshall [a,b,*], Tong Chen [b]

[a] National High Magnetic Field Laboratory, Florida State University, 1800 E. Paul Dirac Drive, Tallahassee, FL 32310, USA
[b] Department of Chemistry and Biochemistry, Florida State University, 95 Chieftain Way, Tallahassee, FL 32306, USA

ARTICLE INFO

Article history:
Received 5 May 2014
Accepted 4 June 2014
Available online 19 July 2014

Keywords:
FT-ICR
FTMS
Penning trap
Stored waveform inverse Fourier transform
SWIFT
MS/MS
Nuclear magnetic resonance
NMR
Orbitrap
Hadamard transform

ABSTRACT

This article reviews the development of Fourier transform ion cyclotron resonance mass spectrometry (FT-ICR MS) in several respects: (a) a strong static magnetic field serves to convert ion mass-to-charge ratio into cyclotron frequency. Because frequency is the most accurately measurable property, ICR MS inherently offers higher mass resolution and mass accuracy than any other mass analyzer. (b) Coherent excitation followed by induced charge detection yields a time-domain signal whose discrete Fourier transform produces a mass spectrum of ions spanning a wide m/z range simultaneously. By simple analogy to weighing objects with a mechanical balance, that "multiplex" advantage can be shown to be equivalent to "multichannel" detection by an array of individual single-channel detectors. (c) FT-ICR MS performance benefits from near-elimination of magnetic field inhomogeneity by inherent ion cyclotron rotation and ion axial oscillation; inherent nearly quadrupolar electrostatic trapping potential and nearly uniform rf electric field homogeneity near the center of the ICR ion trap (both improved even further by recent ICR cell designs); and theoretically optimal excitation and mass selection produced by stored-waveform inverse Fourier transformation (SWIFT). (d) External ion accumulation allows efficient coupling of atmospheric pressure continuous ionization sources (notably electrospray ionization) with pulsed high-vacuum FT-ICR MS excitation/detection, and injection of externally trapped ions through the "magnetic mirror" into the ICR ion trap has been optimized based on ion trajectory simulations. (e) MS/MS can be performed either inside (e.g., electron capture dissociation, infrared multiphoton dissociation) or outside (e.g., collision-induced dissociation, electron transfer dissociation) the ICR ion trap. (f) Finally, FT-ICR MS instrumentation and experimental event sequences have benefited from striking parallels to prior nuclear magnetic resonance spectroscopy developments. Similarly, non-ICR FT MS development (notably the orbitrap) has benefited from FT-ICR precedents.

© 2014 Elsevier B.V. All rights reserved.

1. Introduction

This article represents a personal perspective of the development of Fourier transform mass spectrometry (FT MS), primarily FT ion cyclotron resonance MS. Literature references are therefore illustrative, but not comprehensive. For example, of the dozens of reviews of various stages and aspects of FT-ICR MS technique development and applications, only a few are cited here: early history [1,2], the "teenage" years [3,4], and milestones through the year 2000 [5].

The initial conception of the FT-ICR experiment in 1973 [6] was inspired by analogy to FT-NMR, just as FT-NMR was inspired by prior FT-infrared spectroscopy. It is interesting to note that FT-NMR was introduced [7] almost immediately after the appearance of the Cooley–Tukey fast Fourier transform algorithm [8], which reduced the computational time for discrete Fourier transformation by a factor of (initially) 30 and later 1000. Also, it is not accidental that both FT-ICR MS co-inventors were initially trained as NMR spectroscopists, for reasons that will become clear in Section 2.6.

2. Stages in FT-ICR MS development

2.1. Conversion of ion mass-to-charge ratio to frequency

The first stage in any Fourier transform spectroscopy experiment is to produce and sample a temporal (NMR, MS) or spatial (IR)

* Corresponding author at: National High Magnetic Field Lab., Florida State University, 1800 E. Paul Dirac Drive, Tallahassee, FL 32310, USA.
Tel.: +1 850 644 0529; fax: +1 850 644 1366.
E-mail address: marshall@magnet.fsu.edu (A.G. Marshall).

http://dx.doi.org/10.1016/j.ijms.2014.06.034
1387-3806/© 2014 Elsevier B.V. All rights reserved.

interferogram at equally spaced intervals, so that its discrete Fourier transform yields a frequency-domain spectrum [9]. In mass spectrometry, the property of interest is ion mass-to-charge ratio, m/q, so the first step is to convert m/q to frequency. In the ion cyclotron, that conversion is achieved by placing a moving ion in an applied static magnetic field, B_0, so that the ion rotates at its cyclotron frequency, ω_c:

$$\omega_c = \frac{qB_0}{m} \quad (1)$$

In mass spectrometry, charge is usually expressed as the number, z, of elementary charges (e) per ion, so that Eq. (1) becomes

$$\omega_c = \frac{zeB_0}{m} \quad (2)$$

The principle behind Eq. (1) was first applied in Thomson's 1897 determination of the m/q ratio of the electron [10]. Subsequent stages in ion cyclotron configurations are shown in Fig. 1. Lawrence and Livingston [11] realized that ion cyclotron frequency is independent of ion speed. They therefore formed ions in one of two opposed D-shaped electrodes, with an accelerating electrostatic potential applied between the electrodes. As soon as the ions crossed from one "D" electrode to the other, the sign of the electrostatic potential was reversed, so that when the ions crossed back to the original "D" electrode, they were further accelerated to higher speed. The potential was switched back and forth so as to continue accelerating ions each time they crossed the gap between the two "D" electrodes, thereby achieving acceleration that would otherwise have required a vastly longer (and higher voltage) linear accelerator.

Analytical instruments exploited cyclotron rotation differently. In the "omegatron" (Fig. 1), ions are irradiated by a fixed-frequency rf oscillating electric field in an applied magnetic field. One can think of the linearly oscillating rf field as the sum of two counter-rotating equal-amplitude components, one of which accelerates ions of that cyclotron frequency continuously forward in their orbits while leaving ions of other m/z values unaffected. Thus, "resonant" ions (i.e., ions whose m/z value matches that of the applied rf electric field) spiral outward until they hit a "collector" electrode, and the detected charge is proportional to the number of those ions. By keeping the rf excitation frequency constant, and slowly scanning the applied magnetic field, ions of successively higher m/z could be detected [12]. The omegatron was suitable for "residual" gas analysis (i.e., simple low molecular weight gases).

Wobschall instead measured the power absorption by resonantly excited ions, again at fixed marginal oscillator frequency as the applied magnetic field was swept slowly through resonance (see Fig. 1) [13]. His design was later commercialized by Varian Associates, and applied by John Baldeschwieler's group to measurement of ion–molecule reaction pathways, rates, and equilibria [14]. Baldeschwieler (who also started his independent research career in NMR) realized that cyclotron acceleration of ions of a given m/z ratio could increase their speed (and thus reactivity), and subsequent scanning across the full m/z range provided a means for detecting and quantitating ion–molecule reaction product ions. By analogy to NMR, the experiment was initially called "double resonance" (i.e., initial resonant excitation of reactant ions followed by resonant frequency scanning to detect product ions) [15]. Today, such experiments would be called "tandem" MS or MS/MS, and are typically used to fragment large ions by collisions with inert neutral small gas atoms or molecules (as in gas-phase peptide or protein sequencing).

2.2. Coherent excitation followed by broadband detection: the "multiplex" advantage

FT-ICR MS experiments are conducted at fixed applied magnetic field. Ion cyclotron motion is initially spatially incoherent (i.e., ions are distributed randomly about a small-radius orbit). Coherence is produced by applying an rf oscillating electric field excitation, during which each packet of ions of a given m/z spirals outward to a final orbital radius of a few centimeters. The first FT-ICR MS experiment (Fig. 2) employed a single-frequency rf pulse of duration, T, which could excite ions whose cyclotron frequencies spanned a (narrow) range of $\sim 0.1/T$ Hz (see Fig. 3) [6]. For the next dozen years, broadband excitation was produced by a linear frequency sweep [16,17]. The most versatile excitation is produced by a time-domain voltage generated by inverse Fourier transform of the desired frequency-domain excitation profile (stored waveform inverse Fourier transform, or SWIFT (see Fig. 3)

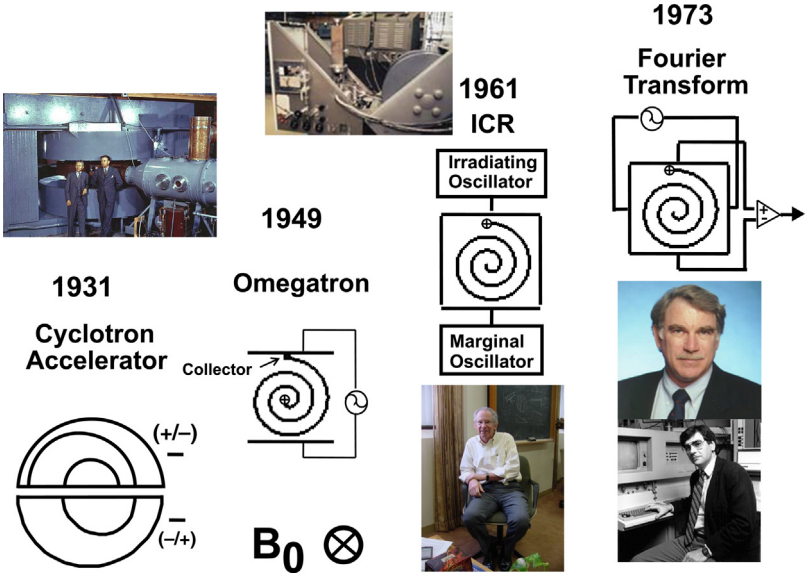

Fig. 1. Stages in cyclotron development history. The individuals shown are Lawrence and Livingston (cyclotron accelerator) [11], John Baldeschwieler (marginal oscillator) [14], and Melvin Comisarow/Alan Marshall (Fourier transform) [6]. Each stage represents a different experimental configuration/event sequence (see text).

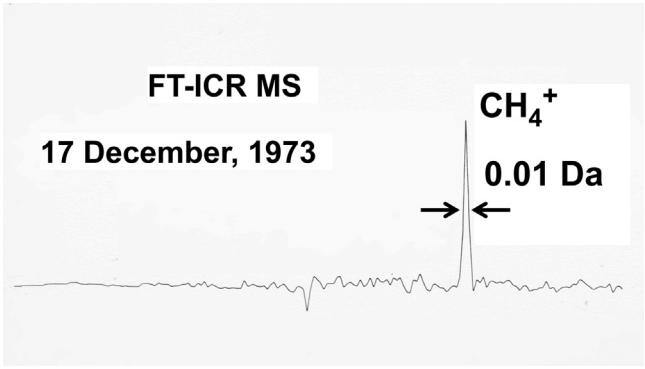

Fig. 2. The first Fourier transform ion cyclotron resonance mass spectrum, produced by electron ionization of methane inside an ICR ion trap [6].

[18,19]. For example, excitation with a flat magnitude spectrum excites ions of a range of m/z values to a common orbital radius. Once ions have reached the specified orbital radius, the excitation is turned off, and the difference in image charge induced by the ions on two opposed electrodes (see below) is converted to a voltage and digitized for subsequent discrete Fourier transformation to yield a frequency-domain spectrum, which is then converted to an m/z spectrum (see below).

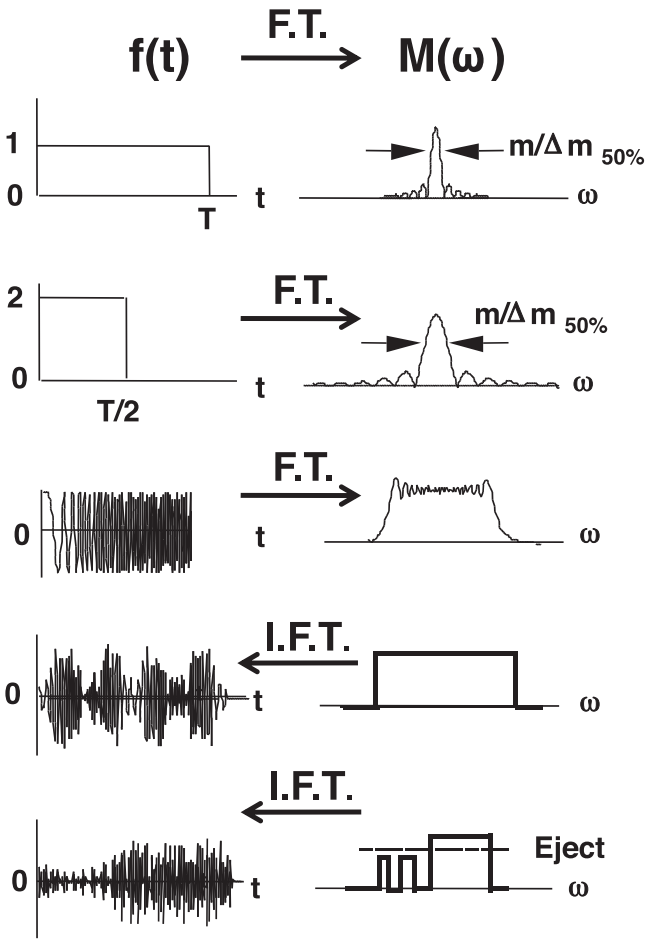

Fig. 3. Time-domain (left) and frequency-domain (right) representations of ICR excitation modes. Top: a rectangular time-domain rf pulse produces frequency-domain excitation that is flat over only a narrow frequency range. Middle: frequency-sweep ("chirp") excitation spans a wide frequency range, but with magnitude ripples. Bottom: stored-waveform inverse Fourier transform (SWIFT) excitation [18,19] produces optimally flat excitation that can include an arbitrary number of zero-magnitude "windows" and/or high-magnitude "ejection" (see text).

The advantages of the FT approach are: (a) ion cyclotron rotation effectively averages out variation in magnetic field (and trapping electric field—see below). That averaging does not occur with the marginal oscillator device, because ions follow a spiral path during detection and never pass through the same spatial point twice. (b) Because the magnetic field is temporally constant (unlike the omegatron or marginal oscillator devices), it can be shimmed to much higher spatial homogeneity for much higher m/z resolving power. (c) Ions of all excited m/z values are detected simultaneously, so that a single m/z spectrum could be obtained ~2000 times faster (or signal-to-noise ratio can be improved by co-adding ~2000 time-domain transients before Fourier transformation) compared to field-scanning single-channel detection.

This last "multiplex" advantage could in principle be achieved by any method for converting N time-domain signal data to N frequency-domain data. It is thus worth understanding what is so special about the Fourier transformation. Consider the problem of determining the unknown masses of N objects with a simple two-pan balance [9]. The most obvious approach is to place each unknown mass, x_i, on one pan of the balance, and then determine the appropriate balancing combination of known mass, y_i, on the other pan. For example, for (say) three unknown masses, the advantage is that no data reduction is required, because each weighing yields one of the unknown masses directly:

$$\begin{aligned} y_1 &= x_1 \\ y_2 &= x_2 \\ y_3 &= x_3 \end{aligned} \tag{3}$$

or, in matrix notation,

$$\begin{pmatrix} y_1 \\ y_2 \\ y_3 \end{pmatrix} = \begin{pmatrix} 1 & 0 & 0 \\ 0 & 1 & 0 \\ 0 & 0 & 1 \end{pmatrix} \begin{pmatrix} x_1 \\ x_2 \\ x_3 \end{pmatrix} \tag{4}$$

However, the measurement is not efficient, because each unknown mass is weighed only once:

Observed weighing result	Unknown mass x_1	x_2	x_3
y_1	1	0	0
y_2	0	1	0
y_3	0	0	1
Number of times each unknown is weighed =	1	1	1

(5)

Ergo, it would be better to put two unknown masses on the balance in each of three different combinations:

$$\begin{pmatrix} y_1 \\ y_2 \\ y_3 \end{pmatrix} = \begin{pmatrix} 1 & 1 & 0 \\ 1 & 0 & 1 \\ 0 & 1 & 1 \end{pmatrix} \begin{pmatrix} x_1 \\ x_2 \\ x_3 \end{pmatrix} \tag{6}$$

Observed weighing result	Unknown mass x_1	x_2	x_3
y_1	1	1	0
y_2	1	0	1
y_3	0	1	1
Number of times each unknown is weighed =	2	2	2

(7)

In this way, each unknown mass is weighed twice, so that the signal-to-noise ratio will be higher by a factor of $2/\sqrt{(2)} = \sqrt{(2)}$ than for one-at-a-time weighing.

Moreover, with this so-called "Hadamard" code (i.e., N unknowns, $N = 2n - 1 = 3, 7, 15$ etc., with $(N+1)/2$ unknowns weighed in each step, such that each row of the code matrix differs from the preceding row by cyclic permutation), the "inverse" code that recovers the unknown masses from the measurements is simply the original code with each "0" replaced by "−1":

$$\begin{pmatrix} x_1 \\ x_2 \\ x_3 \end{pmatrix} = \frac{2}{N+1}\begin{pmatrix} 1 & 1 & -1 \\ 1 & -1 & 1 \\ -1 & 1 & 1 \end{pmatrix}\begin{pmatrix} y_1 \\ y_2 \\ y_3 \end{pmatrix} \tag{8}$$

Finally, it would be even better if all of the N unknown masses could be weighed in each measurement. That is effectively what the Fourier code achieves. For $N = 2n$ equally-spaced samples, $f(t_i)$, of a time-domain signal, the corresponding frequency-domain spectral values, $F(\nu_i)$, are obtained from the Fourier "code", $F_{n,m} = \exp(-i2\pi nm/N)$, $n,m = 0, 1, 2, \ldots, N-1$. For example for a four-point time-domain discrete signal, the corresponding discrete Fourier spectrum is simply:

$$\begin{pmatrix} F(\nu_1) \\ F(\nu_2) \\ F(\nu_3) \\ F(\nu_4) \end{pmatrix} = \begin{pmatrix} 1 & 1 & 1 & 1 \\ 1 & -i & -1 & i \\ 1 & -1 & 1 & -1 \\ 1 & i & -1 & -i \end{pmatrix}\begin{pmatrix} f(t_1) \\ f(t_2) \\ f(t_3) \\ f(t_4) \end{pmatrix} \tag{9}$$

(The mathematically real and imaginary numbers correspond to cosine and sine components (i.e., the "phase") of the (physically real) time-domain signal). Thus, because the magnitude, $|F_{nm}|$, of each term in the Fourier code is unity, it is as if each frequency component is being detected in each time-domain sample—i.e., the equivalent of having N independent single-frequency detectors. A frequency-domain spectrum may thus be obtained in either $1/N$ of the time or with $\sqrt{(N)}$ higher signal-to-noise ratio in the same time as by one frequency-at-a-time scanning. For FT-ICR MS, the time-domain data can be 8 M words or more, so that the "multiplex" advantage is enormous: e.g., ~8.4 million times faster or ~300,000 times higher signal-to-noise ratio.

One can imagine other codes that could convert N time-domain data to N frequency-domain discrete spectral values. However, only the Hadamard and Fourier codes are what mathematicians call "well-conditioned"—i.e., the elements of the "inverse" code (the one that recovers the spectrum from the time-domain signal) do not become unmanageably large. The elements for both Hadamard and Fourier codes have magnitude = 0 or 1. The price to be paid for the conditioning is that the number of code elements is restricted to $(2^n - 1)$ (Hadamard) or 2^n (Fourier).

The Fourier code produces a frequency-domain spectrum in a single matrix calculation. However, (a) it cannot distinguish signal from noise, (b) it requires 2^n equally spaced time-domain data, and (c) spectral peak shape is distorted if the time-domain signal is truncated before it decays entirely to zero. Several other "spectral estimator" methods (autoregression, maximum entropy, "music", filter diagonalization, etc.) based on assumed time-domain signal shape, number of spectral peaks, noise level, etc., can produce frequency-domain spectra that can exhibit narrower apparent peak width. However, those methods are all iterative (i.e., are much slower and can require much more computer memory), and are only as valid as their underlying assumptions. Therefore, FT data reduction is universally preferred in spectroscopy [9].

2.3. Optimization of ion trapping potential and mass calibration/mass accuracy

In retrospect, early FT-ICR MS performance was much better than might have been expected for three reasons. First, the static magnetic field, B_0, confines ions from escaping in directions transverse to B_0, due to ion cyclotron rotation. To prevent positive ions from escaping axially (i.e., along the B_0 axis), a small (~1 V) d.c. potential was applied to each of two flat "end cap" electrodes equidistant from the center of the B_0 field. In fact, the optimal electrostatic trapping potential, Φ_{trap},

$$\Phi_{trap} \propto 2z^2 - x^2 - y^2 \tag{10}$$

for which the cyclotron frequency of an ion is independent of its location inside the trap, would correspond to hyperbolically curved ring and end cap electrodes extending to infinity [20]. Fortunately, the actual electrostatic potential for a tetragonal (i.e., orthogonal with length, L, and a x a square end caps) trap [21],

$$V(x,y,z) = \frac{16V_T}{\pi^2}\sum_{m=0}^{\infty}\sum_{n=0}^{\infty}\frac{(-1)^{m+n}\cos((2m+1)\pi x/a)\cos((2n+1)\pi y)/a)\cosh(k_{mn}\pi\zeta/a)}{(2m+1)(2n+1)\cosh(k_{mn}\pi L/2a)} \tag{11}$$

in which $k_{mn} \equiv \sqrt{(2m+1)^2 + (2n+1)^2}$.

$$V(\rho,z) = 2V_T\sum_{n=1}^{\infty}\frac{J_0(\chi_{0n}\rho/a)\cosh(\chi_{0n}z/a)}{\chi_{0n}J_1(\chi_{0n})\cosh(\chi_{0n}L/2a)} \tag{12}$$

each reduce to the potential for an (ideal) hyperbolic trap as the ion position approaches the center of the trap! Thus, as long as ions are kept near the trap midplane and not excited too far radially outward, the trapping potential would not deviate much from the ideal three-dimensional quadrupolar form of Eq. (10) (Fig. 4, left).

Second, by analogy to spinning the sample in NMR, ion cyclotron rotation (typically at >100,000 Hz) effectively averages azimuthal inhomogeneity in the applied magnetic and electrostatic trapping fields. Similarly, the frequency of ion axial oscillation between the trap end caps is sufficiently high to average axial magnetic field inhomogeneity. Thus, broadband FT-ICR mass accuracy can reach 25 ppb for ions in a magnetic field inhomogeneity of a few ppm [22].

Third, a perfectly quadrupolar electrostatic trapping potential produces an m/z-independent shift in the observed ion cyclotron

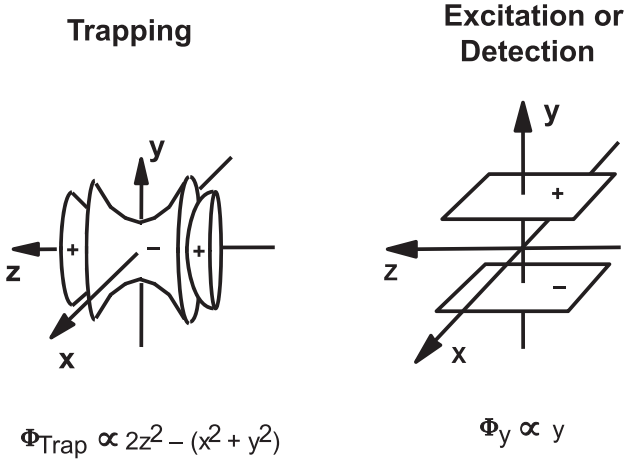

Fig. 4. Theoretically optimal three-dimensional electrostatic quadrupolar trapping potential (left) [20] and theoretically optimal uniform rf electric field excitation potential (right) [90]. All electrodes extend to infinity. The two apparently incompatible requirements may be well approximated by truncating and segmenting the electrodes (see text).

frequency, leading to a two-term equation relating ICR frequency to m/z [23,24]:

$$\frac{m}{z} = \frac{A}{\nu_c} + \frac{B}{\nu_c^2} \tag{13}$$

Thus, it is possible to calibrate an FT-ICR mass spectrum based on measured ICR frequencies for ions of at least two known m/z values, and solving Eq. (13) for the best-fit constants, A and B. However, although ions of a given m/z cannot shift each other's ICR frequency (in a purely quadrupolar trapping potential) [25], Coulomb repulsions between ions of different m/z can produce additional frequency shifts. Fortunately, the electric potential due to such "space charge" has the same approximate functional dependence as Eq. (13) [26]; so that internal mass calibration based on Eq. (13) effectively takes space charge into account. FT-ICR mass calibration can be further improved by modeling the effect of space charge on ions of a given m/z by adding another term based on treating ions of all other m/z as if they were distributed evenly around the cyclotron orbit:

$$\frac{m}{z} = \frac{A}{\nu_c} + \frac{B}{\nu_c^2} + C\frac{\left[\sum_{i\neq j}(M(j))\right]}{\nu_c^2} \tag{14}$$

in which $M(j)$ is the relative magnitude of ions of the jth m/z value. If (as for many complex mixtures), ions of known m/z are widely distributed across the mass spectrum, then an additional improvement is to cut the FT-ICR mass spectrum into (say) 25 segments, and calibrate separately for each segment [22].

2.4. Optimization of ion cyclotron excitation and detection

Ion resonant excitation was initially modeled for a pair of opposed, infinitely extended flat electrodes, for which the rf field is uniform throughout the region between the plates (Fig. 4, right). Truncation and curvature of the electrodes obviously distort the excitation electric field. Moreover, direct computation of the charge induced in detection electrodes is mathematically much more difficult than computation (e.g., by SIMION [27]) of the excitation potential. Fortunately, about a decade after the original FT-ICR MS experiments, Dunbar applied the "reciprocity" principle [28] to ICR, namely, that the differential charge induced between a pair of detection plates by a unit point charge at position, x, is equal in magnitude to the potential (in volts), at position, x, that would be found in the absence of the charge if one detection plate were raised to a potential of 1 V and the other to −1 V [29]. Thus, once one calculates the excitation potential, the same expression will yield the detection signal. Even for simple cell geometries, the expressions for the difference, ΔQ, in charge induced by an ion of charge, q, between two opposed detection electrodes, are formidable:

Tetragonal trap [30]

$$\frac{\Delta Q}{q} = \frac{32}{a^2}\sum_{s=0}^{\infty}\cos((2s+1)\omega_+ t)\sum_{m=1}^{\infty}\sum_{n=0}^{\infty}\sum_{j=0}^{\infty}\frac{m(-1)^{m+n}}{(2n+1)(k'_{mn})^2}\left(1-\frac{\cosh(k'_{mn}z)}{\cosh(k'_{mn}(L/2))}\right)\times\varepsilon_j(-1)^{s+j}J_{2j}\left(\frac{(2n+1)\pi\rho}{a}\right)J_{2(s+j)+1}\left(\frac{2m\pi\rho}{a}\right)$$
$$+\gamma_{j,s}J_{2(s-j)+1}\left(\frac{2m\pi\rho}{a}\right)-\left(1-\gamma_{j,s}\right)J_{2(j-s)+1}\left(\frac{2m\pi\rho}{a}\right) \tag{15}$$

Cylindrical trap [30]

$$\frac{\Delta Q}{q} = \frac{-16}{\pi^2}\sum_{m=0}^{\infty}\sum_{n=0}^{\infty}\frac{\cos((2m+1)\omega_+ t)\sin(((2m+1)\pi/4))\sin(((2n+1)\pi z/L))I_{2m+1}(((2n+1)\pi\rho/L))}{(2m+1)(2n+1)I_{2m+1}((2n+1)\pi a/L)} \tag{16}$$

Fortunately, near the center of either trap, the excitation potential and differential induced change expressions are simply linearly proportional to the radial distance from the B_0 axis (as for a pair of parallel infinitely extended flat electrodes).

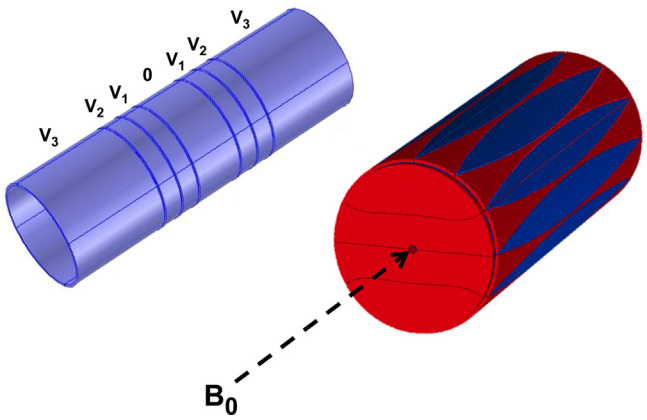

Fig. 5. Seven-section cylindrical (left) [31] and dynamically harmonized (right) [32] ion traps for FT-ICR MS. Each configuration is designed to approximate the optimal three-dimensional quadrupolar trapping potential (Eq. (10) and Fig. 4, left).

Both the electrostatic trapping potential and the rf excitation potential can be "shimmed" to near-perfection by appropriate segmenting of the trap electrodes. Initial FT-ICR ion traps were tetragonal or cylindrical, with flat end caps. Significant improvement in electric potential quadrupolarity was achieved by cutting an open cylindrical trap into several axial segments, and applying appropriate potentials to the various segments (Fig. 5, left) [31]. Quadrupolarity has been further improved by use of multiple quadratically curved "canoe" (grounded) and "hourglass" (d.c. voltage) electrodes (Fig. 5, right) [32]. Although the trapping potential exhibits pronounced discontinuity at each gap, ion cyclotron rotation averages out those discontinuities (hence "dynamic" harmonization).

Major improvement in rf excitation electric field spatial uniformity is achieved by capacitively coupling end cap segments to the central excitation electrodes (see Fig. 6) [33]. Similar improvement for the dynamically harmonized cell is achieved by segmenting the end caps and applying different rf voltage to each segment [34]. Finally, both excitation and detection are improved by widening the azimuthal electrode angle from 90° to 120° (more efficient excitation, as well as stronger detected signal and elimination of 3rd harmonic artifacts) [35]. Of course, the latter approach requires use of the same electrodes for excitation and detection, so additional back-to-back diodes are inserted to isolate the excitation and detection circuits [36].

Until recently, optimal FT-ICR excitation was thought to have a flat magnitude spectrum, because then the detected signal voltage should be independent of m/z. However, if all packets of ions of different m/z traverse the same orbital radius, then ion packets will

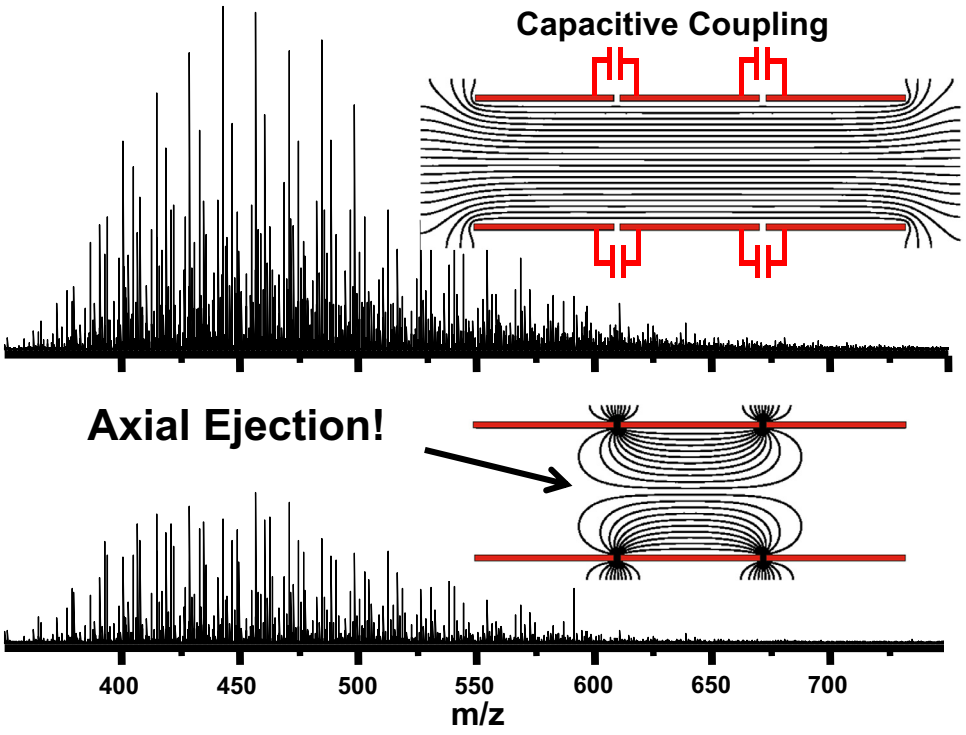

Fig. 6. Single planar electrode pair (bottom) and the same electrode pair capacitively-coupled to each of two end cap electrode pairs (top). The curvature of the rf excitation isopotentials for the single electrode pair produces axial rf excitation leading to m/z-dependent axial ejection. Capacitive coupling of the rf excitation to the end cap electrodes [33] effectively eliminates axial ejection (figure kindly provided by Tanner M. Schaub).

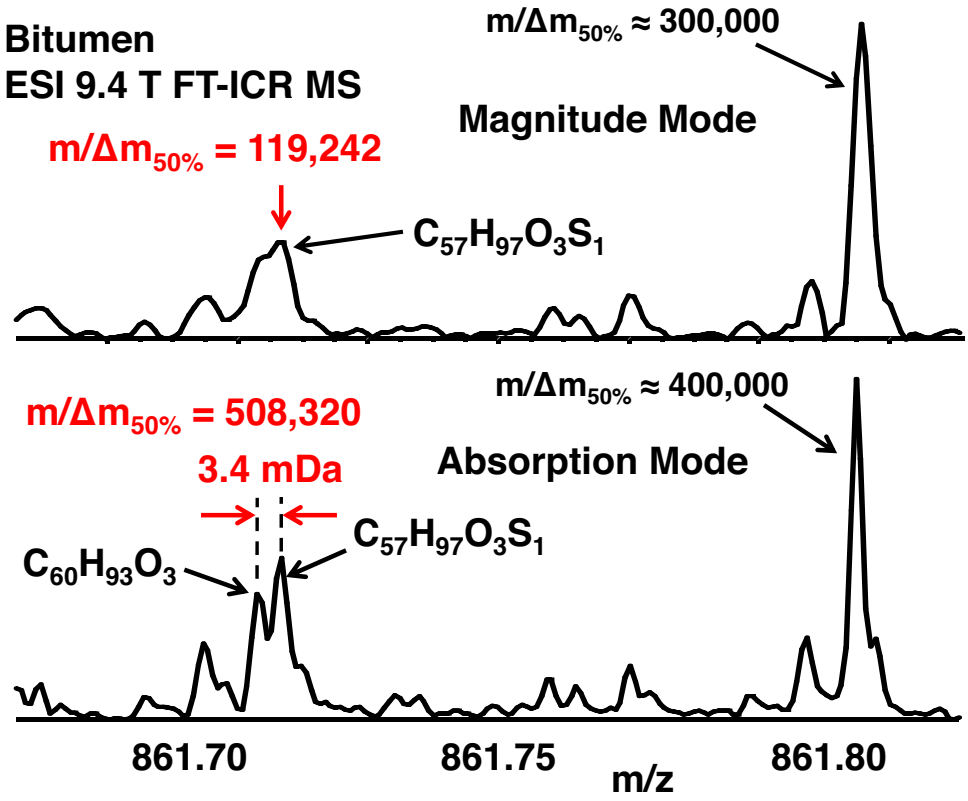

Fig. 7. Magnitude (top) and absorption (bottom) FT-ICR positive-ion mass spectra for electrospray-ionized Athabasca bitumen. Note that even a small increase in mass resolving power provided by phase correction can split a mass doublet that is unresolved in magnitude-mode display [40].

collide periodically, and lower-abundance ion packets will lose coherence faster than higher-abundance ion packets. If the number of coherently orbiting ions falls below the detection threshold, then ions of those m/z values will disappear from the mass spectrum, and dynamic range (i.e., ratio of the highest to lowest magnitude peak) will be reduced. Thus, to maximize dynamic range, it is actually preferable to excite ions of different m/z to different post-excitation ICR radius. The effect is dramatic: e.g., the number of observed FT-ICR MS peaks can be more than doubled by tailoring the ICR post-excitation radii for ions from a complex mixture [37].

Another effect of space charge is that the ICR frequency of a packet of ions of a given m/z value varies according to the total number of trapped ions (see below). For a complex mixture, it is therefore desirable to limit the total number of trapped ions, and co-add many time-domain transients to increase the signal-to-noise ratio. However, an ion source may not necessarily produce the same number of ions for each transient. Therefore, it helps to impose "conditional averaging", by determining the summed magnitudes of all FT-ICR MS peaks for each individual acquisition, and eliminating any acquisitions for which the summed magnitude deviates by more than (say) a few per cent. Conditional averaging can improve mass accuracy by a factor of ~2 [22].

From the outset, it was understood that FT-ICR mass resolving power could be improved by a factor of up to 2 by "phase-correcting" the data to yield an absorption-mode (rather than magnitude-mode) spectrum [38,39]. Over the next 35 years, various attempts at phase correction could succeed for sparse and/or narrow-band spectra, but broadband phase correction has been achieved only recently, based on knowledge of the excitation waveform (see Fig. 7) [40,41].

The cumulative effect of the above manipulations has been an order of magnitude improvement in FT-ICR broadband mass accuracy. Fig. 8 shows the distribution of mass measurement error (i.e., difference between experimental mass and that calculated from the assigned elemental composition) for more than 5000 peaks in an FT-ICR mass spectrum. Systematic error has essentially been eliminated (~5 ppb), and random error has been reduced to less than 30 ppb [22]. It is interesting to note that at this level of accuracy, double-precision (64 bit/word) arithmetic is needed to represent the masses.

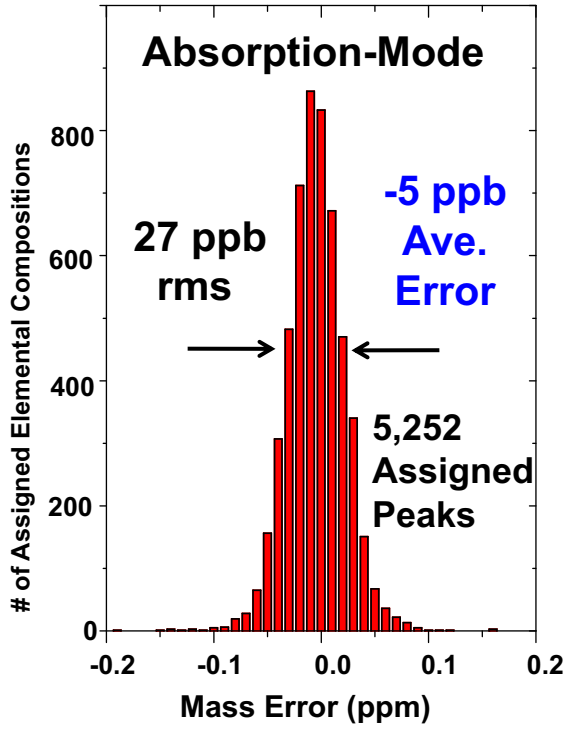

Fig. 8. Mass measurement error distribution for all of the assigned elemental compositions in the FT-ICR mass spectrum for an Athabasca bitumen heavy vacuum gas oil distillate, showing near-elimination of systematic mass measurement error [22].

Finally, considerable insight into the effect of space charge, magnetic and electric field imperfections, and image charge induced by the ions on the side electrodes of the ICR cell has been gained from large-scale (>10^6 trapped ions) simulations of ion trajectories in an ICR trap [42,43]. The dependence of orbiting ion packet coherence on ion number, m/z, trap configuration and size, magnetic field strength, etc., has been characterized, and could help to guide future improvement in ion optics.

2.5. Atmospheric pressure ionization: external ion accumulation and injection into the ICR cell

In the first FT-ICR MS (and most other contemporary mass analyzer) experiments, ions were created by electron ionization in the ICR cell itself. Thus, analysis was limited to analytes with sufficiently high vapor pressure. As analytical applications developed, it became desirable to operate the ICR at the lowest possible pressure, to ensure the longest-lasting time-domain signal and thus the highest frequency- (and m/z-) domain resolving power [44].

As of this writing, most of the major types of ion sources and on-line separators have been interfaced to FT-ICR mass analyzers. In particular, atmospheric pressure electrospray and DART ("direct analysis in real time", based on ionization by metastable helium atoms) produce ions continuously, whereas FT-ICR is an inherently pulsed mass analyzer. Thus, it becomes necessary to accumulate ions in a multiple trap external to the ICR magnet [45]. Ions are then ejected and guided (by multipoles) along the magnetic field axis (to avoid reflection of off-axis ions as they pass through the magnetic field gradient to the ICR cell) [46]. Two immediate problems ensue. First, even if all externally trapped ions are ejected at the same instant with the same kinetic energy, their times-of-flight to the ICR cell will increase with increasing m/z, so that they would not arrive simultaneously. Thus, if the ICR front trap electrode potential is lowered to admit the first (lowest m/z) ions, and if the front trap electrode potential is re-raised to hold them before they can reflect from the back trap electrode and escape, then slower-moving ions of sufficiently high m/z will be prevented from entering the cell. This time-of-flight discrimination can therefore significantly limit the m/z range of trappable ions. Second, if one attempts to eject ions from the external trap by dropping the potential of the external trap end cap closest to the ICR cell and raising the other external trap end cap potential, then the potential inside the external trap will be essentially flat (i.e., no electric field) except at the two ends, and most of the externally trapped ions will leak out slowly, further limiting the number that reach the ICR cell. These problems have largely been solved in two ways. First, a constant voltage applied to angled wires placed between adjacent multiple electrodes of the external trap creates a voltage gradient (and thus an electric field that increases from one end cap to the other). Thus, most of the trapped ions are ejected over short time period, thereby increasing the efficiency of transfer to the ICR cell [47]. Second, application of a secondary rf potential between the two end caps of the external trap creates a pseudopotential well that is deeper for ions of lower m/z. Thus, if the amplitude of the secondary rf potential is ramped steadily downward, ions of highest m/z will be ejected first, and ions of lowest m/z last—appropriate tuning of the ramping rate can effectively compensate for the time-of-flight effect, because

slower-moving ions of higher m/z are ejected first, but will be caught by faster-moving ions of lower m/z ejected last, so that ions of all m/z reach the ICR cell at about the same time. In this way, ions spanning a decade in m/z (e.g., m/z = 200–2000) can be captured with comparable efficiency in the ICR cell [48].

2.6. FT-ICR MS/MS

Initial FT-ICR MS applications were for ion–molecule reaction chemistry, in which reagent ions were created in the ICR cell and mass-selected, after which neutral reagent molecules were injected into the cell, and product ions were identified and quantitated. Thus, these MS/MS experiments were limited to volatile reagents, and mass resolution was typically pressure-limited.

As soon as gas-phase peptide and protein ions could be generated (primarily by ESI and MALDI), gas-phase peptide sequencing proceeded in two ways: (a) slow heating by multiple collisions with low-mass neutrals or by absorption of multiple infrared photons, resulting in breakage of the weakest bond (i.e., the peptide linkage) and (b) capture of a low-energy electron by a multiply-charged peptide cation, resulting in breakage of the N—Cα bond. Although either method can serve for peptide sequencing, electron capture dissociation (ECD), which can be performed only in an ICR cell, had the advantage of retaining post-translational modifications (e.g., phosphorylation, glyscosylation) that are typically cleaved by collision-induced dissociation (CID). Infrared multiphoton dissociation (IRMPD) can also be performed inside an ICR cell. Moreover, ECD can sometimes break an N—Cα bond, but the two fragments remain non-covalently bound; in that case, "activated-ion ECD" with infrared irradiation can separate the fragments, and improve ECD sequence coverage [49].

Even though MS/MS can be performed inside an ICR cell without introducing collision gas, ion fragmentation is increasingly conducted in an ion trap external to the ICR cell, as for CID and the more recently introduced electron transfer dissociation (ETD) [50].

2.7. Parallels: FT-ICR and FT-NMR; FT-ICR MS and FT non-ICR MS

Table 1 lists the impressive number of FT-NMR techniques with exact parallels in FT-ICR MS. Moreover, the historical evolution of FT-ICR MS closely tracks that of FT-NMR. In fact, three aspects of NMR (spinning the sample, frequency-sweep instead of magnetic field sweep, and FT of the time-domain signal following pulsed excitation) occurred separately for NMR, but simultaneously with the advent of FT-ICR MS. Two-dimensional FT/FT NMR spectroscopy is analgous to two-dimensional Hadamard/FT ICR MS [51] and FT/FT ICR MS [52]. Although there is no ICR analog to COSY NMR, NOESY 2D FT/NMR (population transfer of through-space coupled spins) does have an exact analog to 2D FT/FT ICR MS/MS. Just as two protons are coupled through space by dipole–dipole coupling in NMR, precursor and product ions are coupled by chemical reaction in ICR. In each case, a two-dimensional spectrum shows uncoupled spins (precursor ions) on the diagonal, and projections of off-diagonal peaks to the diagonal correspond to through-space coupling (NMR) (or ICR ion–molecule reaction products) between two species [52]. Early attempts at 2D FT/FT ICR MS/MS suffered from what in NMR is called "t_1" noise: namely, streaks in the 2D display rather than sharp peaks, due to variation in the number of ions from one time-domain data acquisition to the next [53]. That effect can be reduced by conditional averaging (see above). If 2D FT/FT can be made robust, then it will become possible to map all possible ion–neutral reactions/fragmentations in a single display.

Fourier transform mass spectrometry may be achieved by various non-ICR methods of converting m/z to frequency. For example, the linear axial oscillation of ions along the applied magnetic field axis in an ICR cell induces a differential charge between the two end caps, and has been used to generate an FT mass spectrum [54]. However, because the axial "trapping" oscillation frequency varies as $1/\sqrt{(m/z)}$ rather than the $1/(m/z)$ variation in FT-ICR resolving power, there is inherently wider frequency dispersion for FT-ICR than for FT axial oscillation mass measurement. By the same token, m/z resolving power is half the oscillation frequency resolving power (much like time-of-flight mass spectrometry, for which the time-of-flight varies as $1/\sqrt{(m/z)}$, so that m/z resolving power is half the time-of-flight resolving power). Finally, mass resolving power for FT axial oscillation varies as $1/\sqrt{(m/z)}$ compared to $1/(m/z)$ for FT-ICR.

FT MS has also been achieved in a quadrupole ion trap (i.e., no applied magnetic field). However, the applied rf electric potential is several orders of magnitude stronger than the differential charge induced between the end caps, so that feedback from the trapping field to the detector could not be eliminated [55]. Moreover, coupling of isotopic peaks was severe, because one ion cloud cannot pass another if both are excited along the same axis. Feedback can be reduced by introduction of a separate small detection electrode embedded in (but isolated from) the adjacent end cap electrode. However, mass resolving power is still limited [56].

Table 1
Conceptual, physical, experimental, and historical analogies between magnetic resonance and ion cyclotron resonance spectroscopies.

NMR and EMR	ICR
Larmor precession (rf freq's)	Ion cyclotron orbital rotation (rf freq's)
Sample spinning	(Automatic due to ion cyclotron rotation)
Rotating frame	Rotating frame [68]
T_1	Ion loss by chemical rxs or radial diffusion
T_2	De-phasing by collisions or space charge
Spin-lock	Ion-lock ("jump" B_0 to zero or double it) [69]
Adiabatic rapid passage	Quadrupolar magnetron/cyclotron conversion [70]
Bloch equations	Quadrupolar excitation [70]
Various spin couplings	Cyclotron/axial/magnetron couplings [71]
Sidebands	Trapping/magnetron sidebands [3]
Double (multiple)-quantum coherence	Double (multiply)-charged ion [72]; harmonics [73]
Shaped (tailored) pulses	Stored waveform inverse FT (SWIFT) [18,19]
Correlation NMR	Correlation ICR [74]; chirp excitation [16,17]
Crossed-coil detection	Orthogonal excitation/detection electrodes [6]
Single-coil detection	Same electrodes for excitation/detection [36]
B_0 shimming	Electrostatic potential shimming [32]
B_1 shimming	rf electric field excitation shimming [33,75]
NOE/population transfer	Ion–molecule reactions [52]
Chemical exchange	Proton transfer reactions
Spin-tickling/double resonance	CID [76], SORI [77], IRMPD [78]
2D NOE/t_1 noise	2D MS/MS, ion number fluctuation noise [52,53]
Hadamard excitation	Hadamard/FT for MS/MS [51]
Quadrature excitation/detection	Quadrature excitation/detection [79]
Spin echo	Ion remeasurement [80]
Radiation damping	Resistive damping [81,82]
Dispersion vs. absorption (DISPA) [83]	Dispersion vs. absorption (DISPA) [84]
Heterodyne detection	Heterodyne or direct detection [9]
FT data reduction	FT data reduction [6]
Non-FT data reduction	Non-FT data reduction [85–87]
Decoupling	Ion ejection [88]
Laser CIDNP	Photodissociation [78,89]

Common history
Field-sweep, frequency-sweep, pulse/FT
Crossed coil, single coil detection
Marginal oscillator power absorption, induced current or charge detection
Single-phase, quadrature detection

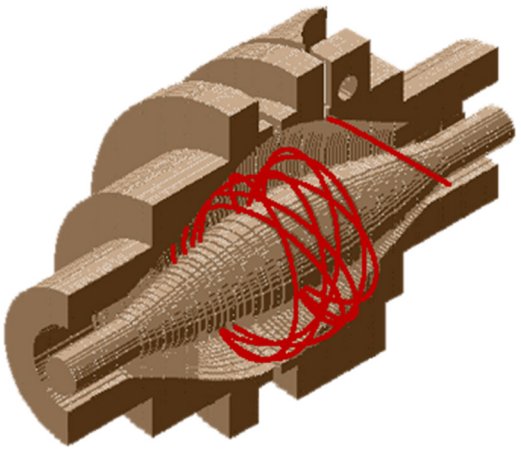

Fig. 9. Schematic diagram of an orbitrap, showing ion injection (upper right) and subsequent ion trajectory. Detection is based on splitting the outer ring electrode at the trap midplane and detecting the difference in charge induced on the two halves. Figure adapted with permission from [91].

FT MS has been performed in a linear electrostatic ion beam trap. However, the detected signal magnitude damped rapidly after a few cycles. Damping could be reduced by "self-bunching" (i.e., appropriate tailoring of the shape of the electrostatic mirror potential), but only for ions of a narrow m/z range [57].

By far the most successful non-ICR FT mass analyzer is the orbitrap [58], in which ions of a wide m/z range are confined in the annulus between two curved electrodes that produce a quadrologarithmic electrostatic potential. Ions oscillate between the two end caps, and also rotate about the central electrode (see Fig. 9) [59]. Detection is achieved by cutting the electrodes at the midplane of the trap, and recording the differential induced change between the two halves. Initial spatial coherence at the moment that ions of a given m/z are injected into the trap is achieved by external storage and ejection of ions from a "C"-shaped quadrupole [60]. Ions of different m/z are injected sequentially, and space charge repulsions are minimized by ramping the potential of the central electrode during injection (sort of like turning up the force of gravity as objects reach the earth, so that they end up parked at different orbital radii). Like the FT axial oscillation in an ICR cell, the orbitrap axial oscillation frequency varies as $1/\sqrt{(m/z)}$, so that frequency dispersion is inherently less than that for FT-ICR MS, and m/z resolving power varies as $1/\sqrt{(m/z)}$ (compared to $1/(m/z)$ for FT-ICR MS). Phase coherence in the orbitrap is much shorter in duration (typically 1.5–3 s) in the orbitrap than for an ICR trap (up to several minutes) [32]. Finally, complete broadband phase correction has not yet been achieved for the orbitrap. The net effect of the above factors is that FT-ICR mass resolving power and mass accuracy are $\sim$10$\times$ higher for FT-ICR MS than orbitrap MS, for ions of m/z <2000. Because orbitrap mass resolving power falls off more slowly with increasing m/z, the difference between FT-ICR MS and orbitrap resolving power decreases with increasing m/z.

Another example of multiplex MS is Hadamard transform time-of-flight MS, in which a continuous ion beam emerging from the ion source is accelerated and then modulated by a pseudorandom sequence of an almost equal number of "on" and "off" pulses. The experiment is then repeated for each of N cyclically permuted pseudorandom sequences (Hadamard-coded), and the data deconvolved with an inverse Hadamard code [61]. The multiplex advantage is approximately half that of multidetection, for significantly improved signal-to-noise ratio. Mass resolution is limited by the difficulty in producing near-instantaneous deflection of ions from "off" to "on", and by m/z-dependent noise. Finally, a similar multiplex advantage has been achieved by Hadamard transform ion mobility mass spectrometery [62,63].

3. Conclusion

40 years of FT-ICR MS development has produced the world's highest mass resolution and highest mass measurement accuracy. With the pending installation of 21 T FT-ICR mass spectrometers at the National High Magnetic Field Laboratory in Tallahassee, FL and Pacific Northwest National Laboratory in Richland, WA, even higher performance is anticipated. Perhaps most important, FT-ICR MS has set the bar that has driven the development and demand for lower (but still high) resolution mass analyzers, notably the orbitrap and multi-pass time-of-flight instruments, for applications ranging from complex mixture analysis [64,65] to peptide/protein sequencing [66] to solution-phase H/D exchange followed by quenching/proteolysis/desalting MS for mapping of contact surfaces in protein complexes [67]. More generally, ultrahigh mass resolving power for identification of unknowns enables subsequent "targeted" analysis with lower-resolution mass analyzers. Thus, state-of-the-art instrumentation benefits a much larger base of users who do not use it directly.

Acknowledgments

This work was supported by the NSF Division of Materials Research through DMR-11-57490, BP/The Gulf of Mexico Research Initiative to the Deep-C Consortium, NIH GM100136-01A1, and the State of Florida.

References

[1] A.G. Marshall, Fourier transform ion cyclotron resonance mass spectrometry, Acc. Chem. Res. 18 (1985) 316–322.
[2] M.B. Comisarow, A.G. Marshall, The early development of fourier transform ion cyclotron resonance (FT-ICR) spectroscopy, J. Mass Spectrom. 31 (1996) 581–585.
[3] A.G. Marshall, P.B. Grosshans, Fourier transform ion cyclotron resonance mass spectrometry: the teenage years, Anal. Chem. 63 (1991) 215A–229A.
[4] I.J. Amster, Tutorial: Fourier transform mass spectrometry, J. Mass Spectrom. 31 (1996) 1325–1337.
[5] A.G. Marshall, Milestones in Fourier transform ion cyclotron resonance mass spectrometry technique development, Int. J. Mass Spectrom. 200 (2000) 331–336.
[6] M.B. Comisarow, A.G. Marshall, Fourier transform ion cyclotron resonance spectroscopy, Chem. Phys. Lett. 25 (1974) 282–283.
[7] R.R. Ernst, W.A. Anderson, Application of Fourier transform spectroscoy to magnetic resonance, Rev. Sci. Instrum. 37 (1966) 93.
[8] J.W. Cooley, J.W. Tukey, An algorithm for the machine calculation of complex Fourier series, Math. Comput. 19 (1965) 297–301.
[9] A.G. Marshall, F.R. Verdun, Fourier Transforms in NMR, Optical, and Mass Spectrometry: A User's Handbook, Elsevier, Amsterdam, 1990.
[10] J.J. Thomson, Cathode rays, Philos. Mag. 44 (1897) 293.
[11] E.O. Lawrence, M.S. Livingston, The Production of high speed light ions without the use of high voltages, Phys. Rev. 40 (1932) 19–35.
[12] H. Sommer, H.A. Thomas, J.A. Hipple, The measurement of e/M by cyclotron resonance, Phys. Rev. 82 (1951) 697–702.
[13] D. Wobschall, Ion cyclotron resonance spectrometer, Rev. Sci. Instrum. 36 (1965) 466.
[14] J.D. Baldeschwieler, ICR spectroscopy, Science 159 (1968) 263–273.
[15] L.R. Anders, J.L. Beauchamp, R.C. Dunbar, J.D. Baldeschwieler, Ion-cyclotron double resonance, J. Chem. Phys. 45 (1966) 1062–1063.
[16] M.B. Comisarow, A.G. Marshall, Frequency-sweep Fourier transform ion cyclotron resonance spectroscopy, Chem. Phys. Lett. 26 (1974) 489–490.
[17] A.G. Marshall, D.C. Roe, Theory of Fourier transform ion cyclotron resonance mass spectroscopy: response to frequency-sweep excitation, J. Chem. Phys. 73 (1980) 1581–1590.
[18] A.G. Marshall, T.-C.L. Wang, T.L. Ricca, Tailored excitation for Fourier transform ion cyclotron resonance mass spectrometry, J. Am. Chem. Soc. 107 (1985) 7893–7897.
[19] S. Guan, A.G. Marshall, Stored waveform inverse Fourier transform (SWIFT) ion excitation in trapped-ion mass spectrometry: theory and applications, Int. J. Mass Spectrom. Ion Process. 158 (1996) 5–37.
[20] H. Dehmelt, Ion traps, Rev. Mod. Phys. 62 (1990) 525–530.
[21] P.B. Grosshans, A.G. Marshall, General theory of excitation in ion cyclotron resonance mass spectrometry, Anal. Chem. 63 (1991) 2057–2061.

[22] J.J. Savory, N.K. Kaiser, A.M. McKenna, F. Xian, G.T. Blakney, R.P. Rodgers, C.L. Hendrickson, A.G. Marshall, Parts-per-billion Fourier transform ion cyclotron resonance mass measurement accuracy with a 'walking' calibration equation, Anal. Chem. 83 (2011) 1732–1736.
[23] E.B. Ledford Jr., D.L. Rempel, M.L. Gross, Space charge effects in Fourier transform mass spectrometry, Mass calibration Anal. Chem. 56 (1984) 2744–2748.
[24] S.D.-H. Shi, J.J. Drader, M.A. Freitas, C.L. Hendrickson, A.G. Marshall, Comparison and interconversion of the two most common frequency-to-mass calibration functions for Fourier transform ion cyclotron resonance mass spectrometry, Int. J. Mass Spectrom. 195–196 (2000) 591–598.
[25] S.-P. Chen, M.B. Comisarow, Simple physical models for coulomb-induced frequency shifts and coulomb-induced in homogenous broadening for like and unlike ions in Fourier transform ion cyclotron resonance mass spectrometry, Rapid Commun. Mass Spectrom. 5 (1991) 450–455.
[26] J.B. Jeffries, S.E. Barlow, G.H. Dunn, Theory of space charge shift of ICR frequencies, Int. J. Mass Spectrom. Ion Process. 54 (1983) 169–187.
[27] D.A. Dahl, SIMION for the personal computer in reflection, version 8.1, Int. J. Mass Spectrom. 200 (2000) 3–25.
[28] W. Shockley, Reciprocity theorem of electrostatics, J. Appl. Phys. 9 (1938) 635.
[29] R.C. Dunbar, The effect of ion position on ICR signal strength, Int. J. Mass Spectrom. Ion Process. 56 (1984) 1–9.
[30] P.B. Grosshans, P.J. Shields, A.G. Marshall, Comprehensive theory of the Fourier transform ion cyclotron resonance signal for all ion trap geometries, J. Chem. Phys. 94 (1991) 5341–5352.
[31] A.V. Tolmachev, E.W. Robinson, S. Wu, H. Kang, N.M. Lourette, L. Pasa-Tolic, R.D. Smith, Trapped-ion cell with improved DC potential harmonicity for FT-ICR MS, J. Am. Soc. Mass Spectrom. 19 (2008) 586–597.
[32] E.N. Nikolaev, I.A. Boldin, R. Jertz, G. Baykut, Initial experimental characterization of a new ultra-high resolution FTICR cell with dynamic harmonization, J. Am. Soc. Mass Spectrom. 22 (2011) 1125–1133.
[33] S.C. Beu, D.A. Laude Jr., Elimination of axial ejection during excitation with a capacitively coupled open trapped-ion cell for FTICRMS, Anal. Chem. 64 (1992) 177–180.
[34] T. Chen, N.K. Kaiser, S.C. Beu, G.T. Blakney, J.P. Quinn, D.G. McIntosh, C.L. Hendrickson, A.G. Marshall, Improving radial and axial uniformity of the excitation electric field in a closed dynamically harmonized FT-ICR cell, Proceedings of the 61st American Society Mass Spectrometry Conference, Minneapolis, MN, 9–13 June, 2013, Poster MP 318, 2013.
[35] C.L. Hendrickson, S.C. Beu, G.T. Blakney, N.K. Kaiser, D.G. McIntosh, J.P. Quinn, A.G. Marshall, Optimized cell geometry for Fourier transform ion cyclotron resonance mass spectrometry, Proceedings of the 57th ASMS Conference on Mass Spectrometry & Allied Topics, Philadelphia, PA, 2009.
[36] T. Chen, S.C. Beu, N.K. Kaiser, C.L. Hendrickson, Optimized circuit for excitation and detection with one pair of electrodes for improved Fourier transform ion cyclotron resonance mass spectrometry, Rev. Sci. Instrum. 85 (2014) .
[37] N.K. Kaiser, A.M. McKenna, J.J. Savory, R.P. Rodgers, C.L. Hendrickson, A.G. Marshall, Tailored ion radius distribution for increased dynamic range in FT-ICR mass analysis of complex mixtures, Anal. Chem. 85 (2012) 265–272.
[38] M.B. Comisarow, A.G. Marshall, Selective-phase ion cyclotron resonance spectroscopy, Can. J. Chem. 52 (1974) 1997–1999.
[39] A.G. Marshall, Convolution Fourier transform ion cyclotron resonance spectroscopy, Chem. Phys. Lett. 63 (1979) 515–518.
[40] F. Xian, C.L. Hendrickson, G.T. Blakney, S.C. Beu, A.G. Marshall, Automated broadband phase correction of Fourier transform ion cyclotron resonance mass spectra, Anal. Chem. 82 (2010) 8807–8812.
[41] F. Xian, Y.E. Corilo, C.L. Hendrickson, A.G. Marshall, Baseline correction of absorption-mode Fourier transform ion cyclotron resonance mass spectra, Int. J. Mass Spectrom. 325–327 (2012) 67–72.
[42] E.N. Nikolaev, R.M.A. Heeren, A.M. Popov, A.V. Pozdneev, K.S. Chingin, Realistic modeling of ion cloud motion in a Fourier transform ion cyclotron resonance cell by use of a particle-in-cell approach, Rapid Commun. Mass Spectrom. 21 (2007) 3527–3546.
[43] G. Vladimirov, C.L. Hendrickson, G.T. Blakney, A.G. Marshall, R.M.A. Heeren, E.N. Nikolaev, Fourier transform ion cyclotron resonance mass resolution and dynamic range limits calculated by computer modeling of ion cloud motion, J. Am. Soc. Mass Spectrom. 23 (2012) 375–384.
[44] A.G. Marshall, M.B. Comisarow, G. Parisod, Relaxation and spectral line shape in Fourier transform ion cyclotron resonance spectroscopy, J. Chem. Phys. 71 (1979) 4434–4444.
[45] M.W. Senko, C.L. Hendrickson, M.R. Emmett, S.D.-H. Shi, A.G. Marshall, External accumulation of ions for enhanced electrospray ionization Fourier transform ion cyclotron resonance mass spectrometry, J. Am. Soc. Mass Spectrom. 8 (1997) 970–976.
[46] R.T. McIver Jr., Trajectory calculations for axial injection of ions into a magnetic field: overcoming the magnetic mirror effect with an R. F. quadrupole lens, Int. J. Mass Spectrom. Ion Process. 98 (1990) 35–50.
[47] B.E. Wilcox, C.L. Hendrickson, A.G. Marshall, Improved ion extraction from a linear octopole ion trap: SIMION analysis and experimental demonstration, J. Am. Soc. Mass Spectrom. 13 (2002) 1304–1312.
[48] N.K. Kaiser, J.J. Savory, C.L. Hendrickson, Controlled ion ejection from an external trap for extended m/z range in FT-ICR mass spectrometry, J. Am. Soc. Mass Spectrom. 25 (2014) 943–949.
[49] M.B. Renfrow, H.J. Cooper, M. Tomana, R. Kulhavy, Y. Hiki, K. Toma, M.R. Emmett, J. Mestecky, A.G. Marshall, J. Novak, Determination of aberrant *O*-glycosylation in the IgA1 hinge region by electron capture dissociation Fourier transform ion cyclotron resonance mass spectrometry, J. Biol. Chem. 280 (2005) 19136–19145.
[50] J.E.P. Syka, J.J. Coon, M.J. Schroeder, J. Shabanowitz, D.F. Hunt, Peptide and protein sequence analysis by electron transfer dissociation mass spectrometry, Proc. Natl. Acad. Sci. U. S. A. 101 (2004) 9528–9533.
[51] E.R. Williams, S.Y. Loh, F.W. McLafferty, R.B. Cody, Hadamard transform measurement of tandem FT mass spectra, Anal. Chem. 62 (1990) 698–703.
[52] S. Ross III, P.B. Guan, T.L. Grosshans, Two-dimensional Fourier transform ion cyclotron resonance mass spectrometry/mass spectrometry with stored-waveform ion radius modulation, J. Am. Chem. Soc. 115 (1993) 7854–7861.
[53] G. van der Rest, A.G. Marshall, Noise analysis for two-dimensional tandem FT-ICR mass spectrometry, Int. J. Mass Spectrom. 208 (2001) 101–111.
[54] L. Schweikhard, M. Blundschling, R. Jertz, H.-J. Kluge, Fourier-transform mass spectrometry without ion cyclotron resonance – direct observation of the trapping frequency of trapped ions, Int. J. Mass Spectrom. Ion Process. 89 (1) (1989) R7–R12.
[55] J.E.P. Syka, W.J. Fies Jr., Fourier Transform Quadrupole Mass Spectrometer and Method, U.S.A. Patent, 1988.
[56] M. Soni, V. Frankevich, M. Nappi, R.E. Santini, J.W. Amy, R.G. Cooks, Broad-band Fourier transform quadrupole ion trap mass spectrometry, Anal. Chem. 68 (1996) 3314–3320.
[57] D. Zajfman, Y. Rudich, I. Sagi, D. Strasser, D.W. Savin, S. Goldberg, M. Rappaport, O. Heber, High resolution mass spectrometry using a linear electrostatic ion beam trap, Int. J. Mass Spectrom. 229 (2003) 55–60.
[58] A. Makarov, Electrostatic axially harmonic orbital trapping: a high-performance technique of mass analysis, Anal. Chem. 72 (2000) 1156–1162.
[59] A.G. Marshall, C.L. Hendrickson, High-resolution mass spectrometers, Ann. Rev. Anal. Chem. 1 (2008) 579–599.
[60] J.V. Olsen, L.M.F. de Godoy, G. Li, B. Macek, P. Mortensen, R. Pesch, A. Makarov, O. Lange, S. Horning, M. Mann, Parts per million mass accuracy on an orbitrap mass spectrometer via lock mass injection into a C-trap, Mol. Cell. Proteomics 4 (2005) 2010–2021.
[61] A. Brock, N. Rodriguez, R.N. Zare, Characterization of a Hadamard transform time-of-flight mass spectrometer, Rev. Sci. Instrum. 71 (2000) 1306–1318.
[62] B.H. Clowers, W.F. Simes, H.H. Hill, S.M. Massick, Hadamard transform ion mobility spectrometry, Anal. Chem. 78 (2006) 44–51.
[63] A.W. Szumlas, S.J. Ray, G.M. Hieftje, Hadamard transform ion mobility spectrometry, Anal. Chem. 78 (2006) 4474–4481.
[64] A.G. Marshall, R.P. Rodgers, Petroleomics: chemistry of the underworld, Proc. Natl. Acad. U. S. A. 105 (2008) 18090–18095.
[65] A.M. McKenna, J.T. Williams, J.C. Putnam, C.M. Aeppli, C.M. Reddy, D.L. Valentine, K.T. Lemkau, M.Y. Kellerman, J.J. Savory, N.K. Kaiser, A.G. Marshall, R.P. Rodgers, Unprecedented ultrahigh resolution FT-ICR mass spectrometry and parts-per-billion mass accuracy enable direct characterization of nickel and vanadyl porphyrins in petroleum from natural seeps, Energy Fuels 28 (2014) 2454–2464.
[66] Y. Mao, S.G. Valeja, J.C. Rouse, C.L. Hendrickson, A.G. Marshall, Top-down structural analysis of an intact monoclonal antibody by electron capture dissociation Fourier transform ion cyclotron resonance mass spectrometry, Anal. Chem. 85 (2013) 4239–4246.
[67] Q. Zhang, L.N. Willison, P. Tripathi, S.K. Sathe, K.H. Roux, M.R. Emmett, G.T. Blakney, H.-M. Zhang, A.G. Marshall, Epitope mapping of a 95 kDa antigen in complex with antibody by solution-phase amide backbone H/D exchange monitored by Fourier transform ion cyclotron resonance mass spectrometry, Anal. Chem. 83 (2011) 7129–7136.
[68] M. Wang, A.G. Marshall, Laboratory-frame and rotating-frame ion trajectories in ion cyclotron resonance mass spectrometry, Int. J. Mass Spectrom. Ion Process. 100 (1990) 323–346.
[69] R. Chen, A.G. Marshall, M. Wang, Ion-locked cyclotron resonance: a means for instantaneously changing ion cyclotron orbital radius, Chem. Phys. Lett. 181 (1991) 168–174.
[70] S. Guan, A.G. Marshall, Bloch equations applied to ICR spectroscopy: broadband interconversion between magnetron and cyclotron motion for ion axialization, J. Chem. Phys. 98 (1993) 4486–4493.
[71] S. Guan, X. Xiang, A.G. Marshall, Axial and radial ion cloud compression: coupling of magnetron and cyclotron motion to axial motion in a segmented cubic FT/ICR ion trap, Int. J. Mass Spectrom. Ion Process. 124 (1993) 53–67.
[72] P.A. Limbach, L. Schweikhard, K.A. Cowen, M.T. McDermott, A.G. Marshall, J.V. Coe, Observation of the doubly charged, gas phase fullerene anions C_{60}^{2-} and C_{70}^{2-}, J. Am. Chem. Soc. 113 (1991) 6795–6798.
[73] P.A. Limbach, P.B. Grosshans, A.G. Marshall, Harmonic enhancement of a dectected ICR signal by use of segmented detection electrodes, Int. J. Mass Spectrom. Ion Process. 123 (1993) 41–47.
[74] R.T. Hunter, R.T. McIver Jr., Correlation ICR, Chem. Phys. Lett 49 (1977) 577.
[75] G.S. Jackson, F.M. White, S. Guan, A.G. Marshall, Matrix-shimmed ion cyclotron resonance ion trap simultaneously optimized for excitation, detection, quadrupolar axialization, and trapping, J. Am. Soc. Mass Spectrom. 10 (1999) 759–769.
[76] R.B. Cody, R.C. Burnier, B.S. Freiser, Collision-induced dissociation with Fourier transform mass spectrometry, Anal. Chem. 54 (1982) 96–101.
[77] J.W. Gauthier, T.R. Trautman, D.B. Jacobson, Sustained off-resonance irradiation for CAD involving FTMS. CAD technique that emulates infrared multiphoton dissociation, Anal. Chim. Acta 246 (1991) 211–225.

[78] D.P. Little, J.P. Speir, M.W. Senko, P.B. O'Cornnor, F.W. McLafferty, Infrared multiphoton dissociation of large multiply-charged ions for biomolecule sequencing, Anal. Chem. 66 (1994) 2809–2815.
[79] J.J. Schweikhard, C.L. Shi, A.G. Marshall, Quadrature detection for the separation of the signals of positive and negative ions in Fourier transform ion cyclotron resonance mass spectrometry, in: L.S.F. Anderegg, C.F. Driscoll (Eds.), Non-Neutral Plasma Physics IV, American Institute of Physics, College Park, MD, 2002, pp. 647–651.
[80] J.P. Speir, G.S. Gorman, C.C. Pitsenberger, C.A. Turner, P.P. Wang, I.J. Amster, Remeasurement of ions using quadrupolar excitation Fourier transform ion cyclotron resonance spectrometry, Anal. Chem. 65 (1993) 1746–1752.
[81] G.-Z. Li, H.S. Kim, S. Guan, A.G. Marshall, Radiatively self-cooled penning-trapped electrons: a new way to make gas-phase negative ions from neturals of low electron affinity, J. Am. Chem. Soc. 119 (1997) 2267–2272.
[82] G.-Z. Li, S. Guan, A.G. Marshall, Sympathetic cooling of trapped negative ions by self-cooled electrons in a Fourier transform ion cyclotron resonance mass spectrometer, J. Am. Soc. Mass Spectrom. 8 (1997) 793–800.
[83] A.G. Marshall, Dispersion vs. absorption (DISPA): a magic circle for spectroscopic line shape analysis, Chemometr. Intell. Lab. Syst. 3 (1988) 261–275.
[84] E.C. Craig, A.G. Marshall, Automated phase correction of FT NMR spectra by means of phase measurement based on dispersion versus absorption relation (DISPA), J. Magn. Reson. 76 (1988) 458–475.
[85] J.E. Meier, A.G. Marshall, Bayesian versus Fourier spectral analysis of ion cyclotron resonance time-domain signals, Anal. Chem. 62 (1990) 201–208.
[86] S. Guan, A.G. Marshall, Linear prediction Cholesky decomposition vs. Fourier transform spectral analysis for ion cyclotron resonance mass spectrometry, Anal. Chem. 69 (1997) 1156–1162.
[87] P.B. O'Connor, V. Mandelshtam, R.T. McIver Jr., Y. Li, Application of filter diagonalization for analysis of FTMS signals, Proceedings of the 47th American Society for Mass Spectrometry Conference on Mass Spectrometry & Allied Topics, American Society for Mass Spectrometry, Dallas, TX, 1999, pp. ThPB017.
[88] L. Chen, A.G. Marshall, Stored waveform mass-selective simultaneous ejection/excitation for Fourier transform ion cyclotron resonance mass spectrometry, Int. J. Mass Spectrom. Ion Process. 79 (1987) 115–125.
[89] R.L. Woodlin, D.S. Bomse, J.L. Beauchamp, Multiphoton dissociation of molecules with low power continuous wave infrared laser radiation, J. Am. Chem. Soc. 100 (1978) 3248–3250.
[90] M.B. Comisarow, FT/ICR spectroscopy, Adv. Mass Spectrom. 7 (1978) 1042–1046.
[91] Q. Hu, R.J. Noll, H. Li, A. Makarov, R.G. Cooks, The orbitrap: a new mass spectrometer, J. Mass Spectrom. 40 (2005) 430–443.